Conf-780213--13

STABLE PHASES IN AGED TYPE 321 STAINLESS STEEL*

J. Bentley and J. M. Leitnaker

Metals and Ceramics Division, Oak Ridge National Laboratory
Oak Ridge, TN 37830

ABSTRACT

X-ray diffraction and Analytical Electron Microscopy have been used to characterize the precipitate phases present in type 321 stainless steel after 17 years of service at ∿600°C. The morphology, crystallography, and orientation relationships with the matrix of the precipitates have been determined along with the chemical composition of several of the phases.

Long-term aging of type 321 stainless steel indicates TiC, not $M_{23}C_6$, is the stable carbide phase. A theory is developed to explain appearance of $M_{23}C_6$ at intermediate times. The theory also indicates the means for preventing $M_{23}C_6$ formation and hence sensitization of the steel to intergranular corrosion. The amount of sigma found correlates well with results from shorter time studies. $Ti_4C_2S_2$ and a complex phosphide-arsenide were also present.

INTRODUCTION

Recently a piece of type 321 stainless steel tubing, which had failed after some 17 years of service between ∿566 and 607°C (1050 and 1125°F) in a superheater of a coal-fired boiler, became available for metallurgical examination. It was part of a failed weld; it had been joined to 2¼ Cr—1 Mo steel by means of Inconel 132 weld metal.

In previous reports [1,2] the examination of this steel was somewhat cursory. There was not a great deal of interest because the failure had occurred between the 2¼ Cr—1 Mo steel and the Inconel 132 weld metal rather than in or adjacent to the type 321 stainless steel. However, titanium-modified steels are of more than passing interest for nuclear applications since these steels seem to have considerable advantages in both mechanical properties and in swelling resistance; and since the steel had been in service for such a long period of time, an in-depth examination was undertaken [3].

*Research sponsored by the Division of Materials Sciences, U.S. Department of Energy, under contract W-7405-eng-26 with Union Carbide Corporation.

DISCLAIMER

Quite recently, Grot and Spruiell [4] examined a titanium-modified type 316 stainless steel aged between 450 and 950°C for periods up to 3000 h and compared its behavior with type 321 stainless steel. However, the aging of a specimen some two orders of magnitude longer under service conditions provides a sort of fiducial point toward which specimens aged for shorter time periods must be proceeding. The present results show that the major phases present after long times are significantly different from those observed in the relatively short-term aging studies of type 321 alloy by Grot and Spruiell [4]. The results are discussed in relationship to alloy design and manufacture.

EXPERIMENTAL

Early examination of the type 321 stainless steel [1,2] revealed extensive dislocation structure in the heat-affected zone near the weld. Consequently, the samples cut for examination were well away from this zone and the dislocation line density was that of an annealed steel. Table 1 gives the gross composition of the type 321 stainless steel determined after its service life, as well as the composition of the steels examined by Grot and Spruiell [4].

Table 1. Composition of Steels (Weight Percent)

C	Cr	Ni	Mo	Ti	Mn	Si	P	As	S	N	Fe
Type 321[a] (this work)											
0.045	18.45	11.93		0.47	1.68	0.69	0.030	0.010	0.015		Bal
Type 321 (Grot and Spruiell)											
0.06	17.48	9.58		0.50	1.69	0.54	0.012		0.006	0.011	Bal
Ti-modified type 316 (Grot and Spruiell)											
0.057	17.52	13.96	2.51	0.29	1.41	0.03	0.005		0.004	0.004	Bal

[a]The analysis was performed after the service life of the element.

Extraction Procedure

Precipitates were anodically extracted from specimens of the type 321 stainless steel tubing at 1.5 ± 0.1 V using a platinum cathode in a 10% HCl—90% CH_3OH solution. Precipitate adhering to the specimen was removed by ultrasonic vibration in CH_3CH_2OH, and the specimen was then dried and weighed. The precipitate was separated from the supernate by centrifuging. The precipitate was washed with CH_3CH_2OH, centrifuged again to separate it from the alcohol, dried in a vacuum desiccator, and weighed. The weights are precise to 30 μg. Possible errors are (1) loss of precipitate through dissolution or inadequate centrifuging and (2) inadequate cleaning of tube or precipitate. Results on carefully prepared alloys have been very consistent, indicating reproducibility within 50 μg. We have never demonstrated that very small precipitates are not being dissolved, but extraction of carbides appears to be a quantitative procedure, within experimental error [5].

X-Ray Procedure

Extracted precipitate specimens were completely dispersed in ethyl alcohol, and the alcohol removed by dropping the dispersion slowly onto a piece

of glass at room temperature. The precipitate was scraped from the glass onto a single crystal wafer of silicon, and a drop or two of ethanol was used to make a paste which was smeared out on the silicon wafer. (The wafer serves as the substrate for the precipitate in a diffractometer and is oriented so that no silicon lines are diffracted to the detector.) A small amount of TaC was dusted on the drying paste as an internal standard. Copper radiation was used, and the beam leaving the specimen was passed through a graphite monochromator to remove any scattered radiation. This procedure resulted in a low background with high sensitivity for phases present in small percentages of the total precipitate. Three to four milligrams of precipitate is sufficient for an x-ray specimen, and from steel it is easy to detect, say, 5% of $M_{23}C_6$ dispersed in a mixture of M_6C and $M_{23}C_6$.

The x rays were detected in a scintillation counter, averaged electronically over a period of 6 s, and the result printed and punched on paper tape. With a scanning rate of 1/8°/min, 80 points were counted and tabulated for each degree (in 2θ). These points were then plotted by machine for examination.

The lattice constant of the steel was obtained on a sliver of steel obtained by electropolishing a cut piece until it reached a fine point. Back-reflection x-ray lines were used and extrapolated by a method described by Vogel and Kempter [6].

Electron Microscopy Procedure

Specimens 3.0 × 3.0 × 0.5 mm were cut from larger pieces by a slow-speed water-cooled diamond saw. They were lightly abraded on a fine SiC paper and subsequently thinned for examination by a two-step process described by DuBose and Stiegler [7].

Carbon extraction replicas were made from specimens used in the electrolytic extraction procedure, described above, and supported on beryllium grids.

Specimens were examined in a JEM 100C (120 kV) analytical electron microscope [8]. Diffraction information was obtained in the conventional Selected Area Diffraction (SAD) mode and elemental analysis was performed using a Kevex 5100 energy-dispersive x-ray spectrometer. Extreme care was taken to eliminate, or correct for, spurious effects in the energy-dispersive x-ray analyses [9]. The method of obtaining quantitative analyses with the energy-dispersive system has been described previously [8,10].

In the identification of precipitate phases by SAD, emphasis was placed on obtaining several low index zones for each of the precipitates. In this regard the eucentric tilting capability of the side-entry double-tilt stage proved to be extremely valuable. Greater ease of and confidence in the identification of the phases result from the use of large d spacings obtained at low index zones. Orientation relationships are also more accurately determined when low index zones of the precipitates are used in connection with the Kikuchi line patterns of the matrix. Problems with double diffraction, which are more prevalent at low index zones, were overcome by inspection, following tilting a few degrees away from the zone about the low index reciprocal lattice vectors.

In the indexing of diffraction patterns fully self-consistent indexing, taking into account the inversion between the Kikuchi map and the corresponding conventional stereogram, was employed [11]. In the indexing on stereograms of non-cubic phases all indices refer to real-space plane normals, unless enclosed in brackets in which case they refer to real-space directions.

X-RAY RESULTS

Table 2 lists the d values and observed peak heights, rather than integrated intensities, of the observed diffraction peaks. The lattice parameters of the fcc TiC phase and the bct σ phase are taken from the diffractometer data in the front reflection region. Also given is the lattice constant of the alloy itself, 3.5912 ± 0.0003 Å.

Table 2. Indexing of Diffraction Data of Precipitate Extracted from Type 321 Stainless Steel[a]

I	d(OBS)	ASTM CARD					
		6-0614, TiC			5-0708, σ[b]		
		(hkl)	a_0	I	d	(hkl)	I
5	2.762[c]						
51	2.495	(111)	4.321	80			
12	2.277				2.261	(002)	10
37	2.222[c]						
65	2.160	(200)	4.320	100			
43	2.127						
45	2.121				2.128	(410)	100
10	2.068				2.063	(330)	80
14	2.020				2.015	(202)	60
33	1.970				1.964	(212)	80
28	1.928				1.928	(411)	100
14	1.882				1.877	(231)	80
8	1.863[c]						
4	1.836				1.830	(222)	10
4	1.761				1.755	(312)	10
8	1.599[c]				1.580	(042)	
6	1.570				1.555	(440)	
32	1.531	(220)	4.330	50	1.531	(332)	
13	1.500						
14	1.307[c]						

[a] Amount of precipitate extracted ranged from 0.55 to 0.37 wt %. Intensities are taken from the indicated ASTM cards. The d values were obtained from Andrews et al. [18]. Values of d and a_0 are in Å. The lattice parameter of the steel was 3.5912 ± 0.0003 Å.

[b] Lattice parameters calculated from observed data for σ phase: $a_0 = 8.807 \pm 0.015$, $c_0 = 4.578 \pm 0.008$.

[c] $Ti_4C_2S_2$ has strong peaks near these d values.

The variation in the amount of precipitate found in multiple extractions is marked (Table 2, footnote a). The usual variation in nonstabilized steels is of the order of 10% or less. The identification of the TiC seems unequivocal. The lattice constant, the relative intensities, and thermodynamic expectations are in accord. The results for sigma phase also seem clear.

The lattice parameters and, of course, the d values of the x-ray diffraction peaks agree with published data. The relative intensities observed do not agree precisely with ASTM Card 5-0708, and the reason for this is not clear.

Strong lines listed for $Ti_4C_2S_2$ by ASTM Card 16-849 are noted also in Table 2, although these cannot be considered to constitute "identification" taken by themselves.

ELECTRON MICROSCOPY RESULTS

Titanium Carbide

The distribution of TiC is shown in Fig. 1. The precipitates are equiaxed with a mean diameter of approximately 250 Å and are often located on dislocations. The diffraction pattern in Fig. 1(c) shows the cube-on-cube orientation relationship. There is good agreement between the TEM results and the x-ray data.

Titanium Carbosulfide

As noted earlier, only tentative identification could be ascribed to $Ti_4C_2S_2$, based on x-ray results. Previous work [12] indicated, however, that alloys with sulfur concentrations as high as the present one showed residual $Ti_4C_2S_2$. Thus, on chemical grounds, it is reasonable to suppose the phase is present. We also found one example of a precipitate of $Ti_4C_2S_2$, shown in the electron micrograph of Fig. 2(a). Figure 2(b) and (c) are SAD patterns of two low index zones which serve to illustrate the type of tilting experiments performed in the identification of the precipitate. The orientation relationship between the precipitate and matrix is shown in the stereogram of Fig. 3.

Energy-dispersive x-ray analysis of the precipitate was also performed. The x-ray spectrum is shown in Fig. 4 and, after necessary corrections [8,9] the composition is shown in Table 3. Of course, carbon is not detectable in this analysis.

Table 3. Results of Quantitative Analysis of $Ti_4C_2S_2$ by Energy-Dispersive X-Ray Spectroscopy[a]

Element	Percent	
	Weight	Atomic
Si	0.15	0.2
S	25.3	34.0
Ti	65.8	59.0
Cr	2.2	1.8
Fe	5.9	4.5
Ni	0.65	0.5

[a]Elements analyzed for were normalized to 100% after determination of relative amounts [8,10].

Sigma

Several distinct sigma phase morphologies were seen (as illustrated in Figs. 5, 7, 8, and 9). Dealing first with intragranular sigma, Fig. 5 shows

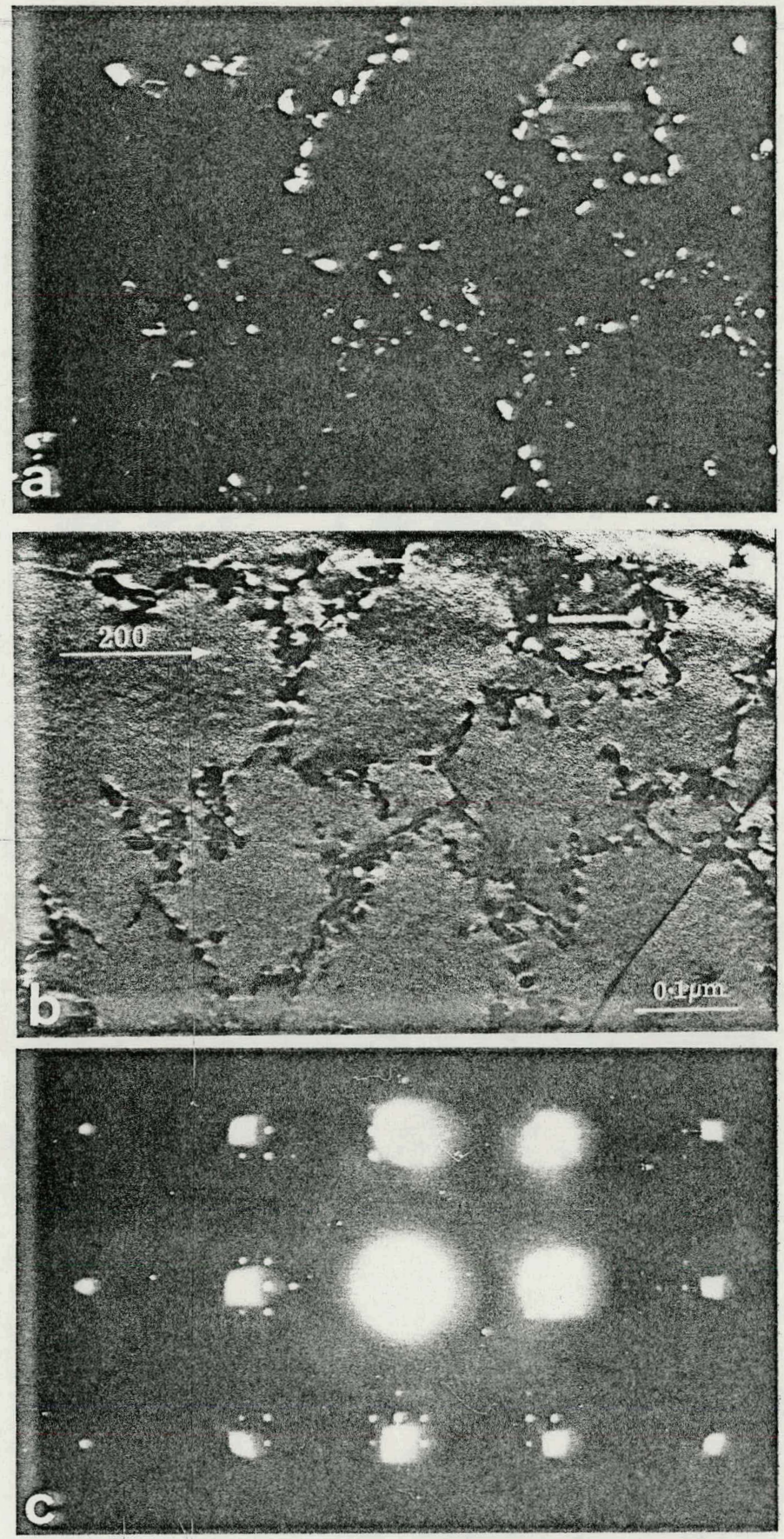

Fig. 1. Titanium Carbide. (a) Dark-field (TiC reflection) micrograph showing distribution of small TiC precipitates. (b) Bright-field micrograph of same area as (a). Comparison shows TiC precipitates are mostly located on dislocations. Beam direction near [001]. Diffracting vector indicated. (c) SAD pattern showing cube-on-cube orientation relationship. All reflections can be accounted for either by direct or double diffraction.

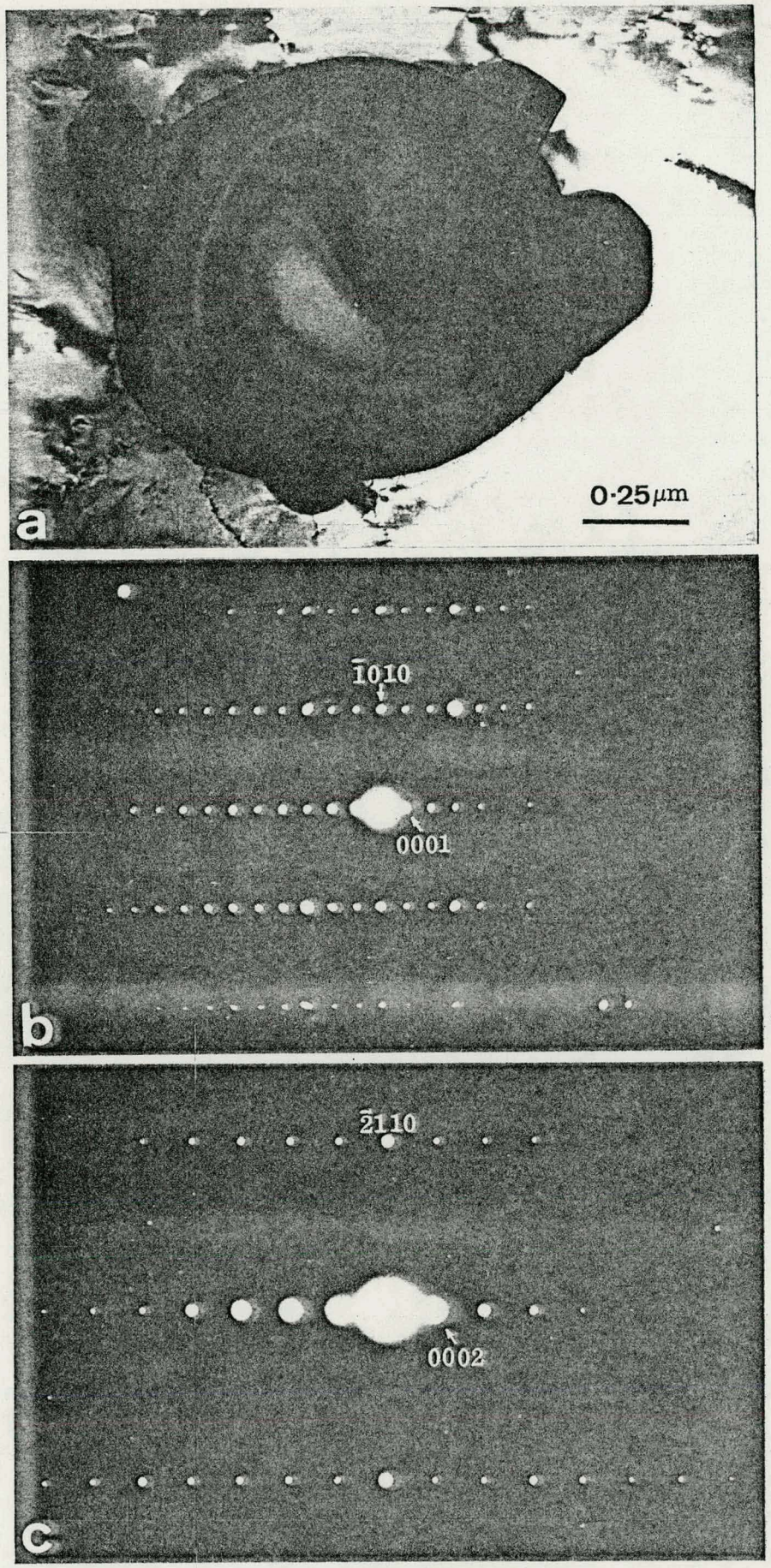

Fig. 2. Titanium Carbosulfide. (a) Micrograph of precipitate, (b) SAD pattern of $[1\bar{2}10]$ zone, (c) SAD pattern of $[0\bar{1}10]$ zone.

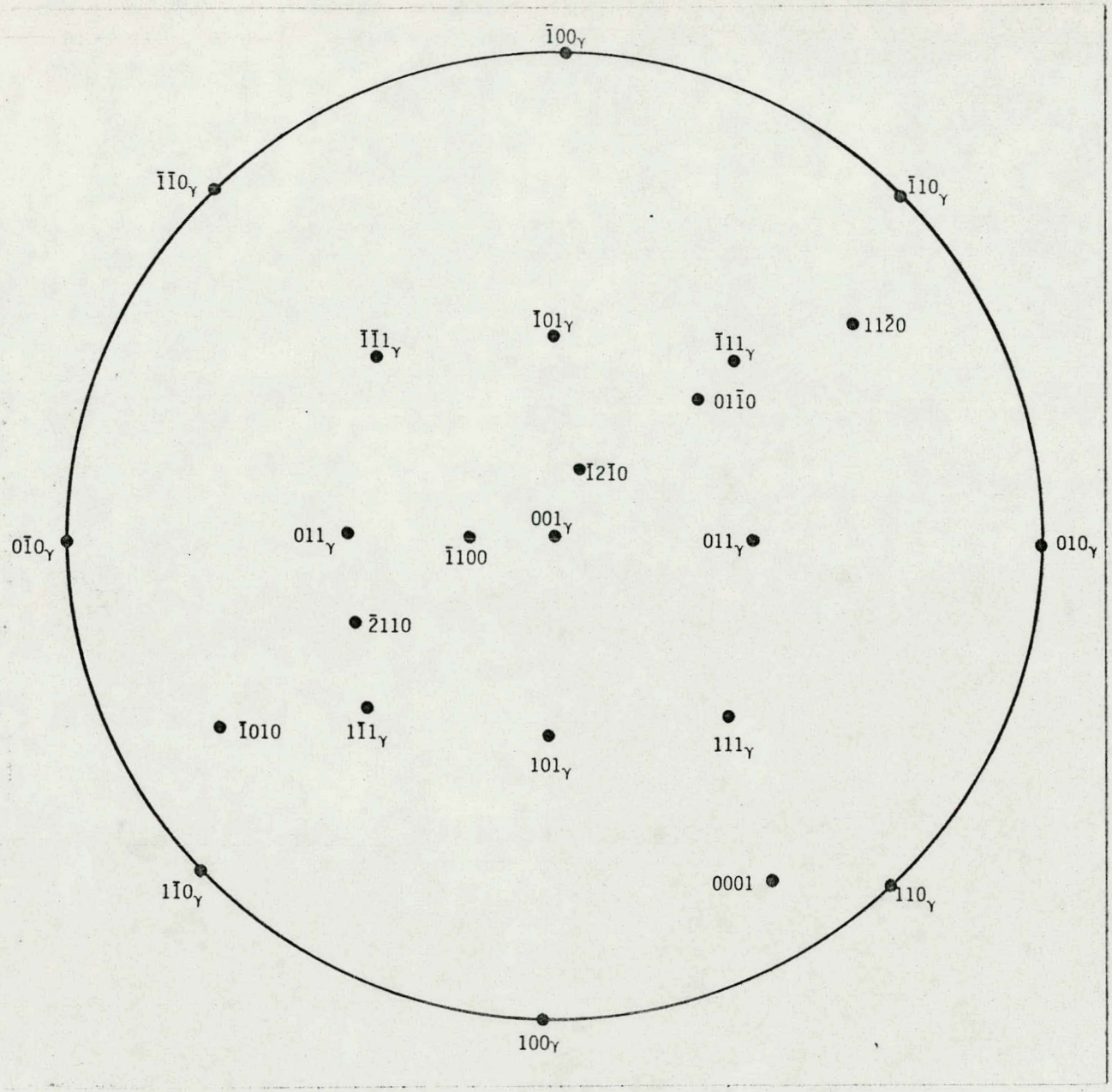

Fig. 3. Stereogram illustrating the orientation relationship of the hexagonal $Ti_4C_2S_2$ precipitate of Fig. 2 with the fcc matrix (γ).

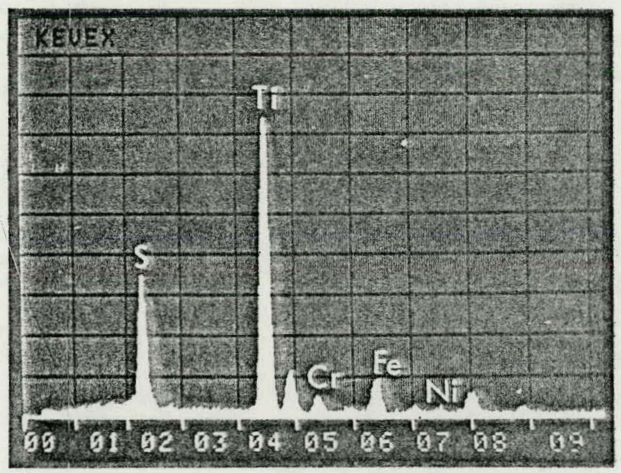

Fig. 4. Energy-dispersive x-ray spectrum of $Ti_4C_2S_2$ precipitate shown in Fig. 2.

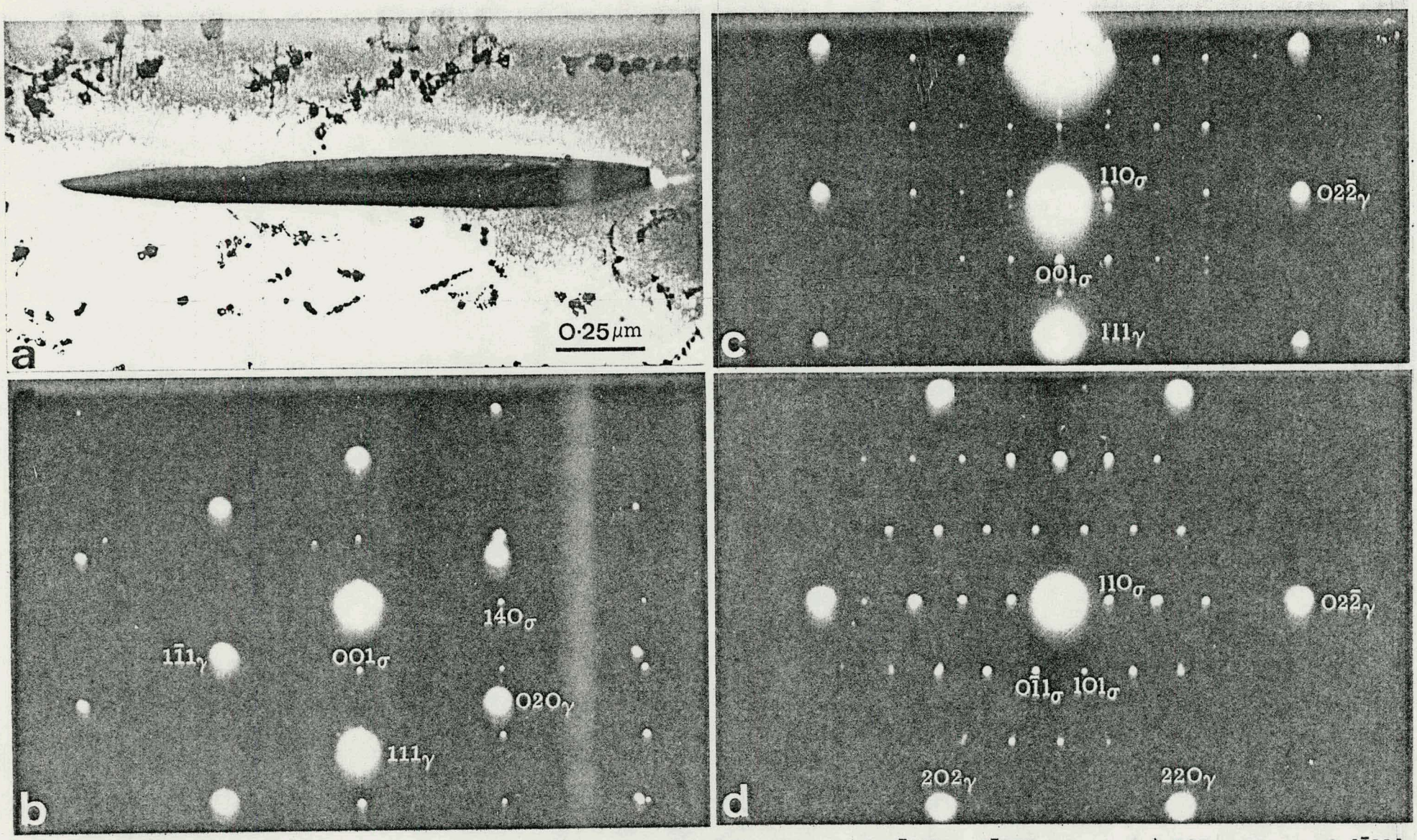

Fig. 5. Sigma I. (a) Micrograph of precipitate. (b) SAD pattern of $[\bar{1}01]_\gamma$, $[\bar{4}10]_\sigma$ zones, (c) SAD pattern of $[\bar{2}11]_\gamma$ $[\bar{1}10]_\sigma$ zones, (d) SAD pattern of $[\bar{1}11]_\gamma$, $[\bar{1}11]_\sigma$ zones.

one fully investigated precipitate. The diffraction patterns of Fig. 5 (b, c, and d) again illustrate the type of tilting experiments performed. The information in these SAD patterns is combined in the stereogram of Fig. 6. The precipitate-matrix orientation relationship may be conveniently described as:

$$(001)\sigma \parallel (111)\gamma$$
$$(110)\sigma \parallel (02\bar{2})\gamma$$

This orientation relationship has also been observed for sigma in type 316 stainless steel by Weiss and Stickler [13]. Note that in Fig. 5(d) the $(\bar{1}1\bar{2})\sigma$ reflection is much more intense than the $(1\bar{1}2)\sigma$ reflection and is consistent with an angular difference of $\sim 0.5°$ between $[\bar{1}11]\gamma$ and $[\bar{1}11]\sigma$. The tilting experiments also revealed that the interfaces of the precipitate with the matrix consisted of:

$$(001)\sigma \text{ , } (111)\gamma \text{ , and } (\bar{1}11)\sigma \text{ , } (022)\gamma$$

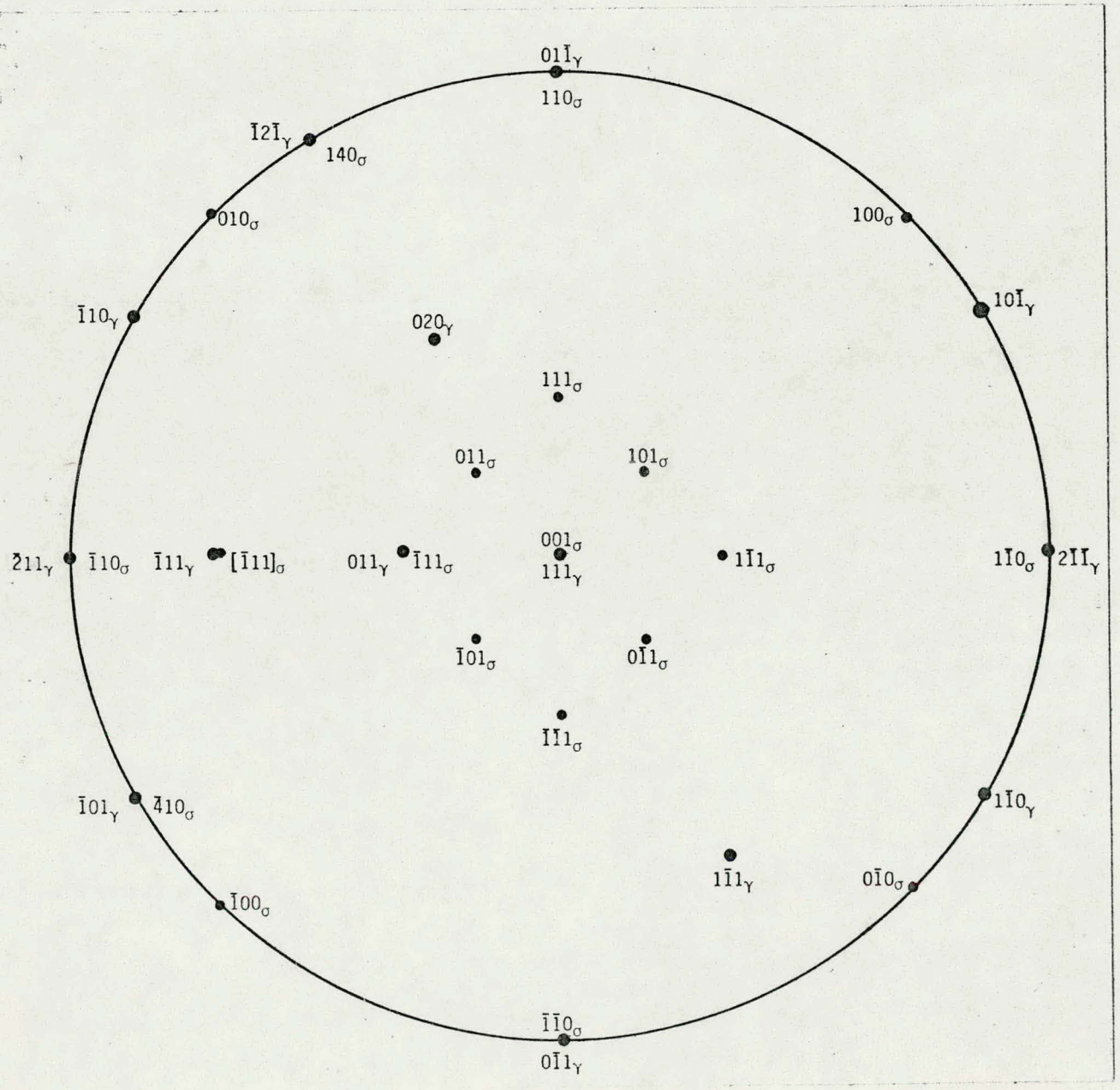

Fig. 6. Stereogram illustrating the orientation relationship of the sigma precipitate of Fig. 5 with the matrix (γ).

Figure 7 shows another example of an intragranular sigma precipitate with the same orientation relationship as in Fig. 6. This precipitate, along with many others observed (including the one shown in Fig. 5) is elongated with a length ≥ 1 μm and a width ~ 0.1 μm.

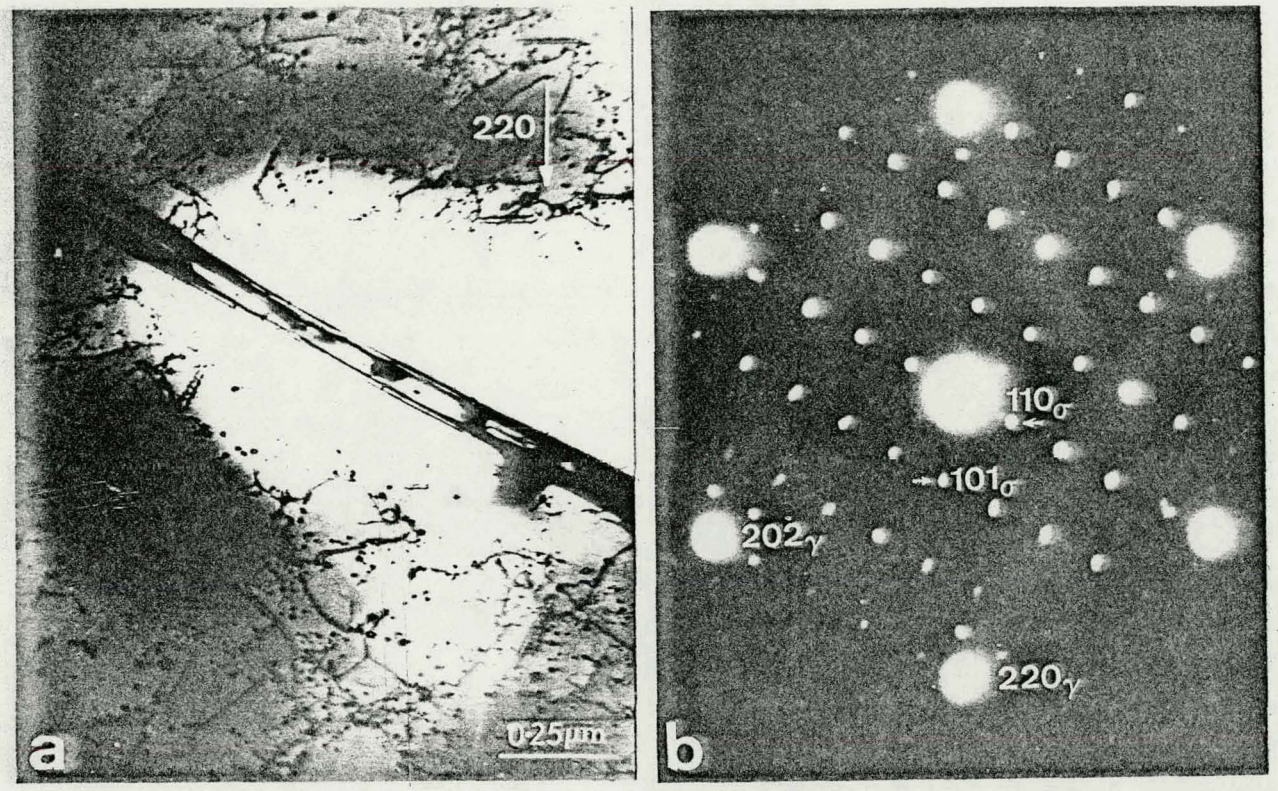

Fig. 7. Sigma II. (a) Micrograph of precipitate. (b) SAD pattern of $[\bar{1}11]_\gamma$, $[\bar{1}11]_\sigma$ zones.

An example of intragranular sigma with a different morphology and orientation relationship is shown in Fig. 8. The orientation relationship may be described as:

$$(\bar{1}\bar{1}1)\sigma \parallel (0\bar{2}2)\gamma$$
$$(1\bar{1}0)\sigma \parallel (2\bar{1}\bar{1})\gamma$$

Again, low-index planes in the precipitate and matrix are parallel, but in this example, unlike the previous examples, the basal plane of the sigma is not parallel to a low-index plane of the matrix. Only one face of the precipitate is crystallographically well-defined and corresponds to $(\bar{1}\bar{1}1)\sigma$, $(0\bar{2}2)\gamma$.

The majority of the sigma phase was observed at grain boundaries. One example is shown in Fig. 9. The intergranular precipitates were much larger than the intragranular sigma, often with dimensions as large as 10 μm. The precipitate-matrix orientation relationships were not investigated in detail, but often some low-index planes in the precipitate and matrix were parallel. For example, in Fig. 9 $(111)\gamma \parallel (011)\sigma$.

Energy-dispersive x-ray analysis of several sigma precipitates was performed. A typical spectrum is shown in Fig. 10. The quantitative results are given in Table 4. Note that the Cr/(Fe+Ni) weight ratio is ~ 0.66 and that there is a non-negligible silicon content.

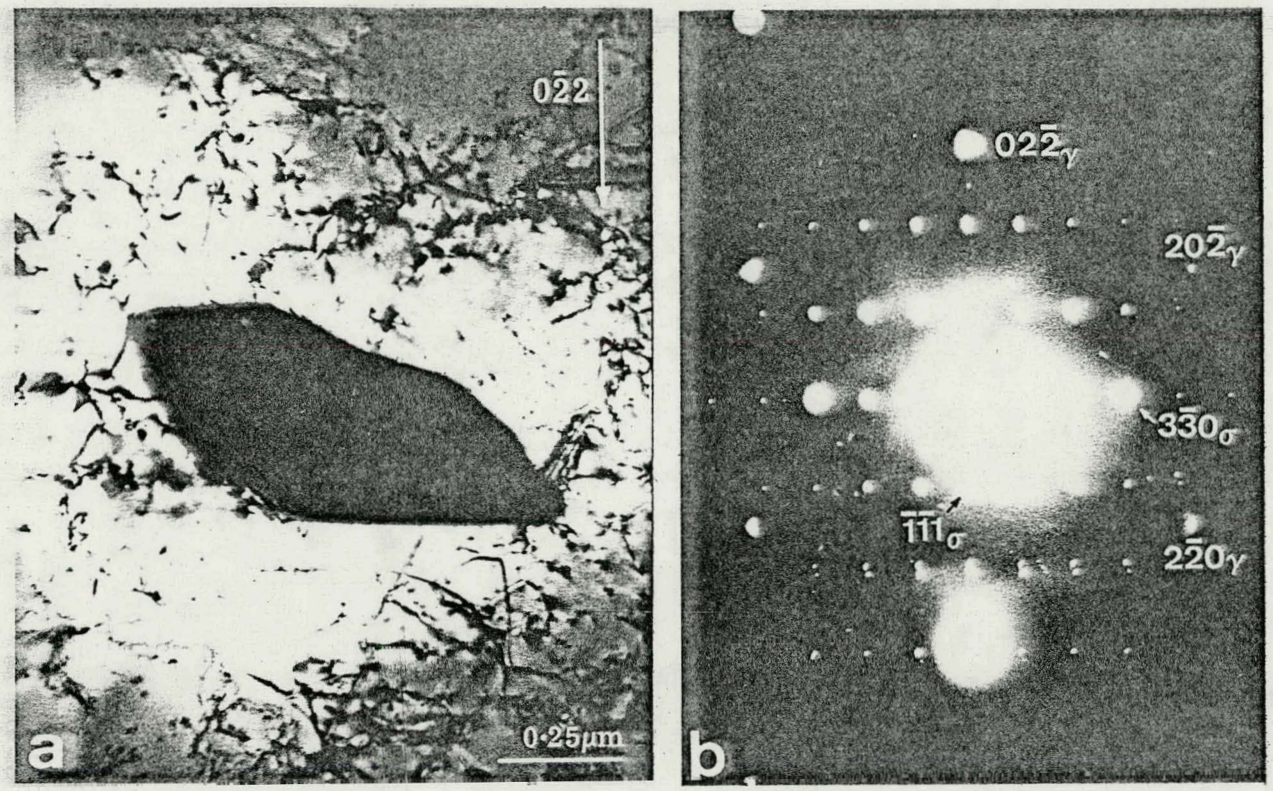

Fig. 8. Sigma III. (a) Micrograph of precipitate. (b) SAD pattern of [111]γ, [112]σ zones.

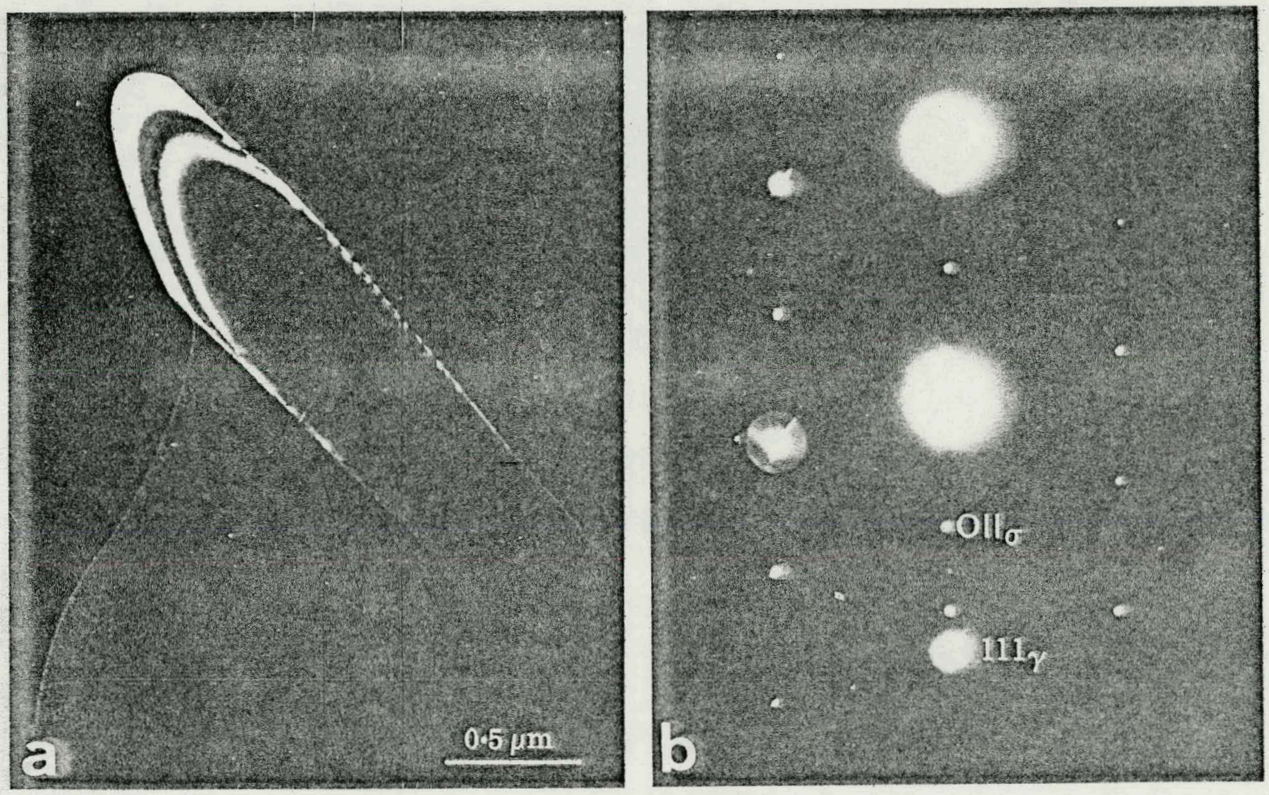

Fig. 9. Sigma IV. (a) Dark-field micrograph of intergranular precipitate. (b) SAD pattern showing (111)γ || (011)σ.

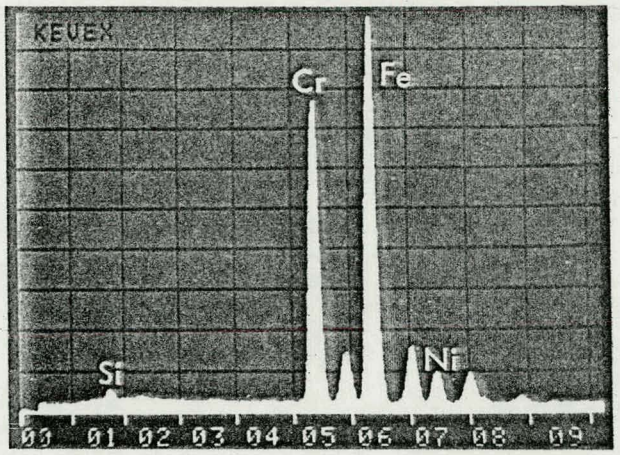

Fig. 10. Typical energy-dispersive x-ray spectrum of sigma phase.

Table 4. Results of Quantitative Analysis of Sigma by Energy-Dispersive X-Ray Spectroscopy[a]

Element	Percent	
	Weight	Atomic
Si	0.9	1.65
S	0.3	0.45
Ti	0.2	0.2
Cr	39.2	40.6
Fe	55.5	53.6
Ni	3.9	3.6

[a]Elements analyzed for were normalized to 100% after determination of relative amounts [8,10].

$M_{23}C_6$

This phase was not seen by x-ray diffraction in this investigation. However, Grot and Spruiell [4] observed it in their investigation of type 321 stainless steel, and the possibility of its occurrence was examined carefully. The precipitate shown in Fig. 8 was initially identified as $M_{23}C_6$. A typical relationship of $M_{23}C_6$ reflections with $(02\bar{2})$ matrix reflections is clearly seen. The intense reflection labeled $(3\bar{3}0)\sigma$ was thought to be {333} $M_{23}C_6$, an intense line in x-ray diffraction, compared with {222} and {111}. A usual relationship, however, for this carbide in steel is shown in Fig. 11. Furthermore, the values of lattice constants calculated assuming $M_{23}C_6$ indexing were not in good agreement. Eventually, the correct identification and indexing [Fig. 8(b)] was obtained.

Complex Phosphide-Arsenide

One further phase was observed in specimen material from the outside of the tube. It was not observed in specimen material from the inside of the tube. The morphology and crystallography are illustrated in Fig. 12. The precipitates are approximately needle shaped with the large dimension along <001> γ. One of the other dimensions is extremely small, of the order of a

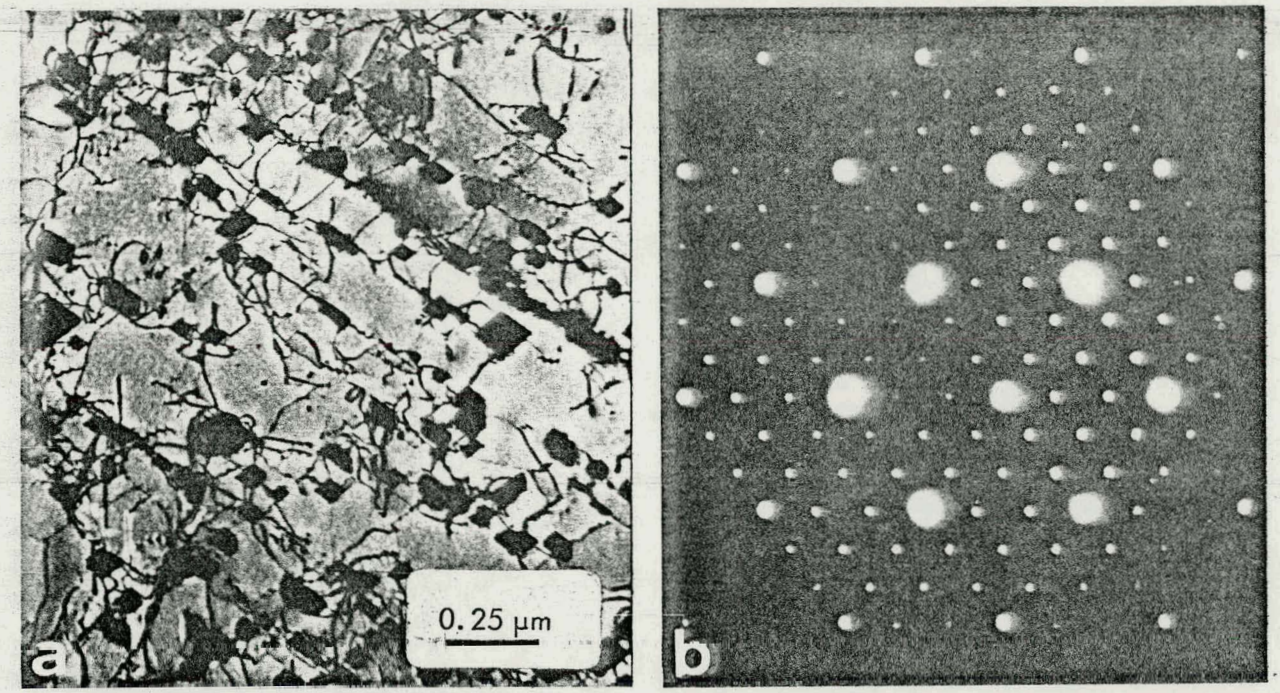

Fig. 11. $M_{23}C_6$ carbide in aged 304 stainless steel. (a) Micrograph. (b) SAD pattern of <110> zone showing cube-on-cube relationship. The steel had been aged 20,000 h at 650°C.

few angstroms, as evidenced by pronounced streaking in the diffraction patterns. The third dimension is ∿200 Å and results in an elongated plate-like precipitate on $\{110\}\gamma$. The precipitates were also frequently observed to exhibit a complex faulted-like internal microstructure. Several SAD patterns are shown in Fig. 12 and illustrate the hexagonal structure of the phase. The orientation relationship between the precipitate and matrix is:

$$(0001)\ \text{precipitate} \parallel (001)\gamma$$

$$(1\bar{2}10)\ \text{precipitate} \parallel (110)\gamma$$

This relationship has a multiplicity of 6. The lattice constants of the phase were determined to be a_0 = 6.08 Å and c_0 = 3.64 Å. The c/a ratio is 0.599; this ratio and structure are consistent with the C_{22} structure of Fe_2P. It is also consistent with an $(Fe,Cr)_2As$ structure identified by Hollan [14].

The elemental composition of the phase was determined by energy dispersive x-ray analysis of isolated precipitates on carbon extraction replicas. Particular care was taken to select precipitates without TiC precipitates in close association. An example of an analyzed precipitates is arrowed in Fig. 13, and the energy-dispersive x-ray spectrum is shown in Fig. 14. The quantitative results of several analyses of different precipitates are given in Table 5.

Apparent differences in morphology, due in large part to variations in foil normals, together with the difficulty of obtaining diffraction information and the multiplicity of habits, resulted in this phase being identified mistakenly as two distinct phases in an earlier report [3].

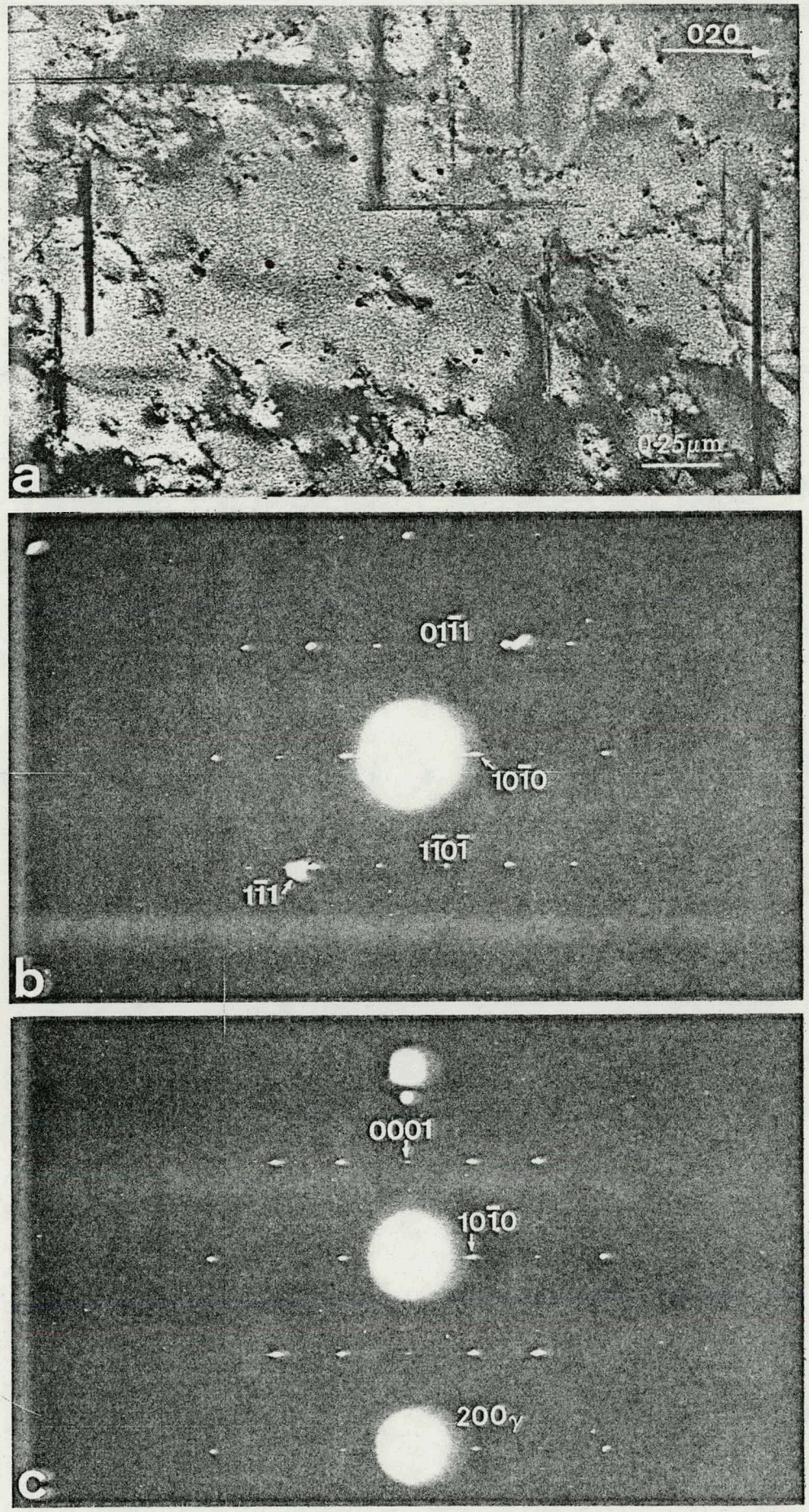

Fig. 12. Rod-shaped phosphide-arsenide precipitates. (a) Micrograph, beam direction near $[001]_\gamma$. (b) SAD pattern of $[1\bar{2}13]$ zone of precipitate, near $[\bar{2}13]_\gamma$. (c) SAD pattern of $[1\bar{2}10]$ zone of precipitate, near $[013]_\gamma$.

Fig. 13. Bright-field micrograph of carbon extraction replica showing rod-shaped complex phosphide-arsenide precipitates and small TiC precipitates.

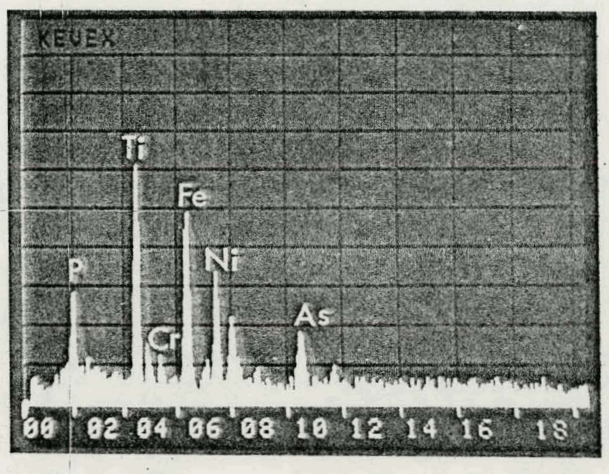

Fig. 14. Energy-dispersive x-ray spectrum of the precipitate arrowed in Fig. 13.

Table 5. Results of Quantitative Analysis of Extracted Hexagonal Phosphide-Arsenide Phase by Energy-Dispersive X-Ray Spectroscopy[a]

Element	Percent	
	Weight	Atomic
P	7.3	12.5
Ti	27.0	29.9
Cr	3.8	3.9
Fe	27.0	25.7
Ni	17.1	15.4
As	17.8	12.6

[a]Elements analyzed for were normalized to 100% after determination of relative amounts [8,10].

DISCUSSION

After 17 years of service, the precipitate phases in this particular type 321 stainless steel are primarily TiC and sigma phase. These constitute the major phases, but $Ti_4C_2S_2$ as well as a complex phosphide-arsenide are present in minor quantities. The phases $M_{23}C_6$ and chi were not seen in these steels, either by x-ray or electron diffraction. We discuss the implications of the observations phase by phase.

$Ti_4C_2S_2$

Previous work [12] revealed the presence of this phase in titanium-modified type 316 stainless steel in material heated at 1200°C and quenched. From the weight of precipitate extracted, the previous work showed that one could account for essentially all the sulfur in the steel. By assuming that no more than 10% of the sulfur remained in solution at 1200°C, a limit was set on the heat of formation of TiS (bound as the carbosulfide) as more negative than −79 kcal/mole.

The results of the energy-dispersive x-ray analysis indicate that, for the present isolated example (although Cr, Fe, and Ni are present in small amounts) the metal/sulfur ratio is very close to the expected stoichiometric value. There appears to be no rational orientation relationship between the precipitate and matrix, perhaps not surprising, if as expected, the precipitate formed from the melt at very high temperatures. There appears to be no doubt that essentially all the sulfur is bound in this phase.

TiC and $M_{23}C_6$

These phases will be discussed together, even though only TiC was observed in this work. The initial purpose of adding titanium to austenitic stainless steels was to prevent sensitization to intergranular corrosion [15]. The mechanism of sensitization is believed to be depletion of chromium from the grain boundaries by formation of $M_{23}C_6$. Early work by Rosenberg and Darr [15] on sensitization showed that the Ti/C weight ratio is an important factor in preventing sensitization, but the previous history was also shown to be important. For example, for a Ti/C weight ratio of 7, a treatment of 0.5 h at 982°C (1800°F) of the as-received material was enough to prevent sensitization, while 3 min at 1080°C (1975°F) of the same material permitted significant grain boundary attack.

Grot and Spruiell [4] observed $M_{23}C_6$ in their type 321 stainless steel samples aged between 450 and 950°C for periods up to 3000 h. After short-time aging $M_{23}C_6$ was clearly the major phase revealed by x-ray examination of the extracted precipitate. (They had given a final grain size control anneal at 1093°C, but the time involved and the previous history of the steel is not known.)

After an in-service age of 17 years, no $M_{23}C_6$ is seen in the presently studied alloy. Since the titanium and carbon contents in the present material and the type 321 stainless steel examined by Grot and Spruiell are almost identical, one concludes that TiC is stable relative to formation of $M_{23}C_6$. Since the formation of TiC does not appear to be inhibited kinetically, some explanation is needed to account for the variation in sensitization seen [15], the formation of $M_{23}C_6$ in Grot and Spruiell's type 321 alloy [4,16], and the relationship to the formation of TiC.

During thermomechanical treatment of titanium-modified alloys, the MC-type precipitates are frequently agglomerated into stringers, as shown in Fig. 15. When such materials are heated to high temperatures the stringers disappear, but on reaging they appear at approximately the same place. This observation has been interpreted [17] to indicate that slow-moving elements, *e.g.*, titanium, remain in the vicinity of the stringers while fast-moving elements, *e.g.*, carbon, are dispersed. The concept of a fast-moving carbon and slow-moving titanium provides a simple explanation for the apparent discrepancy between the present work and that of Grot and Spruiell as well as for scatter in intergranular corrosion data:

Consider two adjacent volumes in steel, *A* and *B*. Volume *A* has a lot of precipitation; volume *B* has none. The steel is heated to a "solution annealing" temperature, whereupon the carbide in volume *A* dissolves. However, only the carbon is dispersed relatively evenly between *A* and *B* during the short heat treatment; the active metal (*e.g.*, titanium) remains in *A*. During the subsequent rapid cooling, the carbon does not have time to rejoin the active metal in volume *A*, but remains relatively evenly distributed through both *A* and *B*. The carbon thermodynamic activity immediately after cooling is high in both *A* and *B*. In volume *A* the carbon rapidly reacts during sensitization treatment with titanium. In volume *B* too little titanium is present and the carbon reacts with chromium, forming $M_{23}C_6$ at grain boundaries and causing sensitization of the alloy. Thus, while under equilibrium conditions enough titanium would have been present to completely react with the carbon, removing it to a very low level, under a commonplace set of processing conditions, as described above, kinetic factors permit the formation of $M_{23}C_6$.

Such a set of conditions can explain the discrepancy in the presently examined sets of data. Also explained is why two investigators might obtain different results for nominally the same composition of material. If the prior processing histories of the materials differed significantly, one might well see varying degrees of sensitization. That is, if most of the TiC were

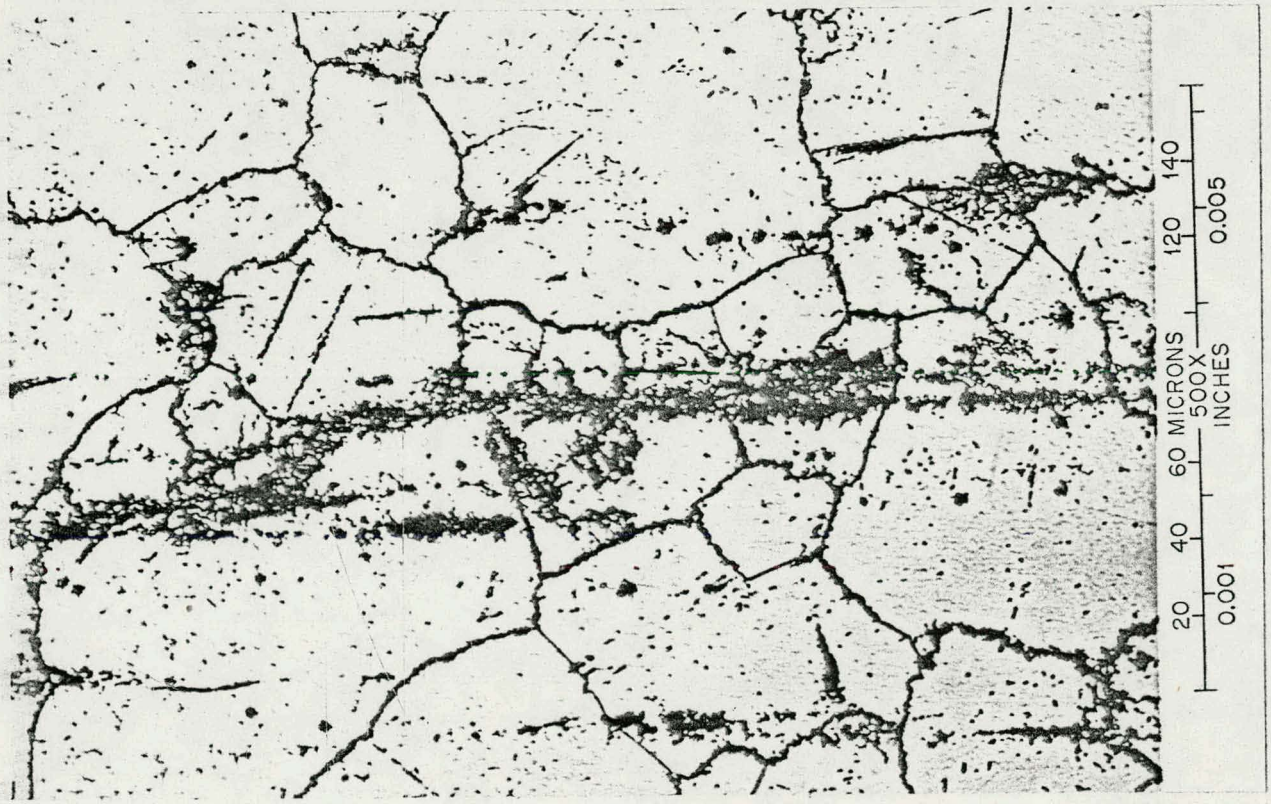

Fig. 15. Typical "stringers" of MC-type precipitates in titanium-modified nickel-base alloy (Hastelloy N).

precipitated out during the thermomechanical treatment prior to the final "solution annealing" one should expect more sensitization than for a more homogeneously distributed material. Reexamination of the previously examined type 321 stainless steel alloy by Spruiell [16] revealed that it was indeed inhomogeneous, as required by the present model.

According to the above explanation, the amount of titanium required to prevent sensitization with a given carbon content is seen to be dependent on previous history, and experimentally this is observed. For example, see Figs. 3 and 4 of the early work by Rosenberg and Darr [15]. There is both the experimental variation — even within a fairly closely controlled investigation — and the strong dependence on previous history. (Some, but not all, of the variability can be accounted for by the variation in nitrogen content of the alloys, as noted in the discussion of that paper.) Therefore, in principle, one cannot know if a particular specimen can be sensitized without either knowing the previous history of the specimen or performing an experiment.

A metallurgical procedure for optimizing "stabilized" alloys has recently been given by Braski and Leitnaker [17]. Briefly, it consists of ensuring that the alloy receives its thermomechanical treatments so as to minimize the segregation of MC-type carbides.

One final point worthy of emphasis in this section concerns the observed fine distribution of TiC. Seventeen years at ~600°C is not sufficient to cause significant agglomeration, indicating that any beneficial effects are essentially permanent.

Sigma

This phase has been clearly identified, both by x-ray and by electron diffraction. The lattice parameters found, $a_0 = 8.807 \pm 0.015$ Å and $c_0 = 4.578 \pm 0.008$ Å are close to those reported by Andrews et al. [18]. The statistical error is larger than it should be because of drift in the diffractometer. The subsequent use of TaC as an internal standard on the specimens has eliminated the problem, but there did not appear to be any strong reason to repeat the work.

The morphologies seen are varied and the orientation relationships with the matrix are also varied. Weiss and Stickler [13] have previously noted the varying orientation relationship between matrix and sigma phase in type 316 stainless steel and, furthermore, reported that frequently the orientation relationship shown in the stereogram of Fig. 6 could be identified. However, Weiss and Stickler [13] also state that sigma does not nucleate homogeneously in the austenite matrix but always requires a high energy interface for nucleation. Our observations, while certainly showing that sigma is nucleated and grows most readily at grain goundaries and other interfaces, also reveal that significant nucleation and growth of sigma can occur in the austenite matrix without the presence of high energy interfaces.

This and other investigations show that there is no single fixed orientation relationship between the sigma phase and the austenite matrix, and one concludes that there is little difference in free energy among a number of sigma-matrix orientations. However, a careful inspection of the observed orientation relationships described earlier in the section entitled *Electron Microscopy Results*, reveals that there is always a close match of both direction and *d* spacing, between at least one set of planes in the precipitate and one set of planes in the matrix. Significant matches for several low-index planes which are observed to be parallel are shown in Table 6. Thus, in the

Table 6. Orientation Relationships Between Sigma Phase and Matrix

Matrix (γ)	Sigma (σ)	Ratio of Plane Spacings d_σ/d_γ
{220}	{110}	~5
{220}	{111}	~3
{111}	{011}	~2

orientation shown in Fig. 6 several sets of $\{220\}\gamma$ are parallel to $\{110\}\sigma$ or $\{111\}\sigma$; in the orientation shown in Fig. 8 one set of $\{220\}\gamma$ is parallel to $\{111\}\sigma$; and in the orientation shown in Fig. 9 one set of $\{111\}\gamma$ is parallel to $\{011\}\sigma$. Of course, many more higher index planes can also be matched — for example, in Fig. 5 $(d_{413})\sigma \approx (d_{220})\gamma$ and $(d_{1\bar{1}2})\gamma \approx 3(d_{422})\gamma$, but those in Table 6 are considered to be the most important.

The growth of sigma phase contrasts strongly with the growth of both $M_{23}C_6$ and TiC. The carbides bear a strong relationship with the matrix. Both appear to nucleate easily and grow rapidly. Sigma nucleates with difficulty — at least it is slow doing so — and grows slowly.

As regards the composition of the sigma phase, one point is worthy of comment. The present Cr/(Fe+Ni) weight ratio of 0.66 compares favorably with (Cr+Mo)/(Fe+Ni) weight ratios of 0.67 and 0.71 obtained by Weiss and Stickler [13] and work at our laboratory, respectively, both for sigma in type 316 stainless steels. Weiss and Stickler [13] used energy-dispersive x-ray analysis in a SEM, and we used analysis of an electrolytic extraction solution together with the weight fraction of precipitate and the original composition of the alloy.

The presence of sigma phase in an alloy generally allows fracture to occur more easily. Embrittlement of a steel has been related quantitatively to an "equivalent Cr content" by Hull [19] and the embrittlement was believed to have been caused primarily by the formation, during aging at 810°C, of the intermetallic phases, sigma and chi.

The amount of sigma formed in the steel examined can be calculated as follows:

1. First calculate the wt % $Ti_4C_2S_2$ from the wt % of S (Table 1) as 0.066 wt %.
2. Second calculate the wt % of TiC from the remaining C, after $Ti_4C_2S_2$ is formed: 0.185 wt %.
3. Finally the wt % sigma is then the (average) total wt % precipitate, 0.46, less the other two major constituents, or 0.21 wt % sigma, of which approximately 40% is Cr. Thus, a reduction of about 0.08 ± 0.05 wt % in the Cr content of the steel should eliminate the sigma phase entirely.

It is useful to compare the present steel quantitatively with those previously examined, for the importance of these embrittling phases can hardly be overemphasized. There are a number of relationships which have been worked out relating the composition to the sigma formation. Note that the overall metallurgical problem is not just finding how much Cr is to be removed in a specific alloy to prevent sigma formation. Rather the problem is to describe the stable boundary of the austenite phase in N-dimensional phase space, where N is the number of elements in the steel. A recent attempt was the equation of Hull [19]. (The Hull description was derived in terms of embrittlement, as noted previously.) Hull [20] has noted there is a great deal of scatter in his final equation covering 11 elements. But the variation for a single element, say Ni, in a system after 1000 h at 816°C is exceedingly small (see Hull's Fig. 3). Since the difference between the alloy treated here and that of Grot and Spruiell is essentially only the difference in Ni and Cr, Hull's equation is a good approximation. We subtracted out the Ti

forming TiC and $Ti_4C_2S_2$ to compare an "equivalent Cr"* nature of 17.97 wt % for the present alloy with the 17.31 wt % for Grot and Spruiell's type 321 stainless steel. Thus the results are seen to be consistent. Grot and Spruiell would not be expected to see sigma phase since their "equivalent Cr" content lies more than ∿0.08 wt % Cr below ours, and they do not.

The amount of Cr (or "Cr equivalent") which must be removed to prevent sigma formation is exceedingly small and is actually within experimental error of chemical analysis for Cr. The point is not so much that 17.9 wt % "Cr equivalent" is the precise limit as that a precise limit exists. In type 321 stainless steel this value (17.9) can be used with reasonable confidence. The reason for the scatter in the "Cr equivalent" value as a variety of elements are included in the Hull equation is undoubtedly interaction of one solute element on another. That is, the effect on sigma formation of Mo addition varies not only with the Mo itself but also with how much Cr is present. For precise results over widely varying compositions of several elements, that is, within the uncertainties of chemical analyses, interaction parameters of at least some of the element pairs will have to be included.

Complex Phosphide-Arsenide

The implications of the presence of the phosphide-arsenide phase are difficult to assess. The region in which the phase was clearly identified was in the outside of the tube. Thus, its presence may be related to the service conditions of the particular material under investigation. Recently, however, a similar precipitate has been identified in neutron-irradiated type 316 stainless steel [21].

In addition to the more general effects that the precipitates may have on the mechanical properties of the steel, the presence of phosphorus, arsenic, and a significant amount (∿30%) of titanium in the phase may have important consequences. Since the volume fraction of the phase is difficult to measure, a reliable estimate of the amount of phosphorus and arsenic bound in this phase cannot be obtained. However, it appears likely that a considerable portion of the 300 wt ppm of phosphorus and 100 wt ppm of arsenic may be bound in this phase.

SUMMARY AND CONCLUSIONS

1. The precipitate phases observed in this alloy are TiC, $Ti_4C_2S_2$, sigma and a complex phosphide-arsenide.

2. The long-time aging (17 years) implies equilibrium is more closely attained than in previous work and that TiC — not $M_{23}C_6$ — is the stable carbide phase.

3. A mechanism is developed to explain precipitation of $M_{23}C_6$ by thermomechanical segregation of TiC, followed by dissolution of the carbide and dispersion of the C, but not the Ti.

4. The TiC does not agglomerate in 17 years at ∿600°C, indicating any beneficial effects are essentially permanent.

---

*Cr equivalent = Cr + 0.31 Mn + 1.76 Mo + 0.97 W + 2.02 V + 1.58 Si + 2.44 Ti + 1.70 Nb + 1.22 Ta − 0.226 Ni − 0.177 Cr.

5. The varied morphology of the sigma phase is in accord with previous examinations.

6. The amount of sigma accords well with previous examinations at much shorter times.

ACKNOWLEDGMENTS

The authors would like to thank Drs. J. O. Stiegler, E. A. Kenik, and P. S. Sklad for manuscript reviews and Frances Scarboro for manuscript preparation.

REFERENCES

[1] GRAY, R. J., KING, J. F., LEITNAKER, J. M., and SLAUGHTER, G. M., *Examination of a Failed Transition Weld Joint and the Associated Base Metals,* ORNL-5223 (January 1977).

[2] GRAY, R. J., KING, J. F., LEITNAKER, J. M., and SLAUGHTER, G. M., *Proceedings of the Ninth Annual Technical Meeting of the International Metallographic Society,* (eds., FILER, E. W., HOEGFELDT, J. M., and McCALL, J. L.), American Elsevier Publishing Co., Inc., New York, NY, 1977.

[3] LEITNAKER, J. M. and BENTLEY, J., *Met. Trans.* 8*A*, 1605–13 (1977)

[4] GROT, A. S. and SPRUIELL, J. E., *Met. Trans.* 6*A*, 2023–30 (1975).

[5] LEITNAKER, J. M., KLUEH, R. L., and LAING, W. R., *Met. Trans.* 6*A*, 1949–55 (1975).

[6] VOGEL, R. E. and KEMPTER, C. P., *Acta Cryst.* 14, 1130–34 (1961).

[7] DuBOSE, C.K.H. and STIEGLER, J. O., *Semiautomatic Preparation of Specimens for Transmission Electron Microscopy,* ORNL-4066 (February 1967).

[8] CARPENTER, R. W., BENTLEY, J., and KENIK, E. A., *Scanning Electron Microscopy* 1, 410–22, 1977, IIT Research Institute, Chicago, Illinois.

[9] KENIK, E. A., and BENTLEY, J., *Proceedings of 35th Annual Meeting of Electron Microscopy Society of America,* pp. 328–29, 1977, Claitor's Publishing Division, Baton Rouge, Louisiana.

[10] CLIFF, G. and LORIMER, G. W., *J. Microscopy* 103, 203–7 (1975).

[11] LORETTO, M. H. and SMALLMAN, R. E., *Defect Analysis in Electron Microscopy,* Chapman and Hall, London, 1975.

[12] LEITNAKER, J. M. and GEHLBACH, R. E., *Thermodynamics of Precipitation Reactions in Titanium-Modified Stainless Steel,* ORNL-TM-4543 (July 1974).

[13] WEISS, B. and STICKLER, R., *Met. Trans.* 3, 851–66 (1972).

[14] HOLLAN, L., *Ann. Chim.* 1, 437–48 (1966).

[15] ROSENBERG, S. J. and DARR, J. H., *Trans. ASM* 41, 1261–1300 (1949).

[16] SPRUIELL, J. E., Department of Chemical and Metallurgical Engineering, University of Tennessee, Knoxville, private communication, 1977.

[17] BRASKI, D. N. and LEITNAKER, J. M., *Production of Homogeneous Titanium-Hastelloy-N Alloys,* ORNL-TM-5697 (1977).

[18] ANDREWS, K. W., DYSON, D. J., and KEOWN, S. R., *Interpretation of Electron Diffraction Patterns,* 2nd. ed., p. 216, Plenum Press, New York, NY, 1971.

[19] HULL, F. C., *Weld. Res.*, 52, 104–13 (1973).

[20] HULL, F. C., Westinghouse Research Laboratories, Pittsburgh, PA, private communication, 1977.

[21] BENTLEY, J., Oak Ridge National Laboratory, Oak Ridge, TN, unpublished research, 1978.